Measurement of two-dimensional small rotation angles by using orthogonal parallel interference patterns

Xiaoli Dai, Osami Sasaki, John E. Greivenkamp, and Takamasa Suzuki

Based on measuring one-dimensional small rotation angles by using a parallel interference pattern (PIP), a method for measuring two-dimensional (2D) small rotation angles by using two different PIP's that are orthogonal to each other is proposed. We simultaneously measure the 2D small rotation angles $\Delta\theta$ and $\Delta\phi$ by detecting the phases of the orthogonal PIP's reflected by an object at two detection points. A sensitivity of 4.9 mrad/arcsec and a spatial resolution of 1.5×1.5 mm^2 are achieved in the measurement. Theoretical analysis and experimental results show that error ε_1 in the measurement of $\Delta\phi$ is almost equal to $-0.01\Delta\theta$ and error ε_2 in the measurement of $\Delta\theta$ is almost equal to $-0.01\Delta\phi$. For small rotation angles of less than a few tens of arcseconds, the random errors whose standard deviations are 0.6 arcsec are dominant.

Key words: Two-dimensional small rotation angles, orthogonal parallel interference patterns, interferometry.

1. Introduction

When two collimated laser beams intersect a small angle, a parallel interference pattern (PIP) occurs. In our previous paper,[1] we described a method for measuring one-dimensional small rotation angles by using a PIP. In this paper, we develop a method for measuring simultaneously two-dimensional (2D) small rotation angles by using two different PIP's that are orthogonal to each other. The methods that use a Michelson interferometer[2–4] and an autocollimator[5,6] can also be used to measure 2D small rotation angles. However, as described in our previous paper,[1] the low spatial resolution of these methods cannot be avoided. The methods using a Michelson interferometer have a trade-off between spatial resolution and angular sensitivity. The method, by using a PIP, does not have this trade-off. The spatial resolution is determined by the period space of the PIP. The sensitivity depends on the period space of the PIP and the positions of the two detection points at which the phases of the PIP are detected. We can obtain a high sensitivity by adjusting the positions of the two detection points. So, it is significant that the method, by using a PIP, is developed to measure 2D small rotation angles. A sensitivity of 4.9 mrad/arcsec and a spatial resolution of 1.5×1.5 mm^2 are achieved in our measurement.

In Section 2 we generally analyze a parallel pattern reflected by an object to obtain the phase changes on the two detection points resulting from the rotation of the object. From the results in Section 2, we determine two kinds of incident PIP to measure independently two angles of 2D rotation in Section 3. When the necessary alignments of the incident PIP's and the object given in Section 3 are not done exactly, we have measurement errors. We analyze these errors in detail in Section 4. We describe the characteristics of our method in Section 5. In Section 6 we present an experimental setup in which we use sinusoidal phase-modulating interferometry and a feedback control system to eliminate the effects of mechanical vibrations. In Section 7 we examine how the errors appear in the measurement of 2D rotation angles and show that the theoretical analysis of our method is supported by experimental results.

X. Dai is with the Graduate School of Science and Technology, Niigata University, Niigata 950-21, Japan. O. Sasaki and T. Suzuki are with the Faculty of Engineering, Niigata University, Niigata 950-21, Japan. J. E. Greivenkamp is with the Optical Sciences Center, University of Arizona, Tucson, Arizona 85721.

Received 5 December 1995; revised manuscript received 4 March 1996.

0003-6935/96/285657-10$10.00/0

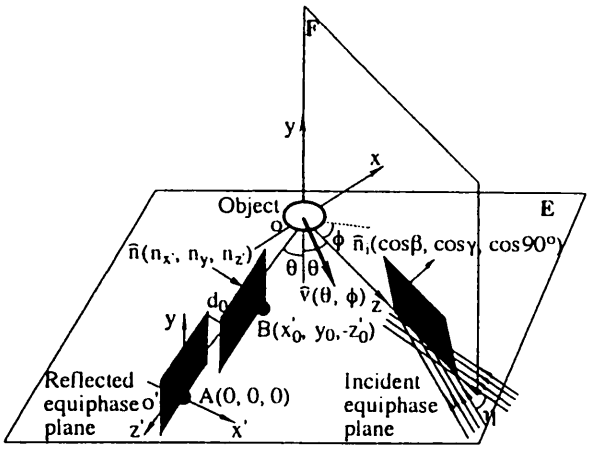

Fig. 1. Reflection of a parallel interference pattern.

2. Reflection of a Parallel Interference Pattern

As shown in Fig. 1, a PIP occurs when two collimated laser beams intersect a small angle η. The PIP consists of some alternating dark and bright planes between which the phase changes from 0 to 2π. We define an equiphase plane as the plane on which the phases of the PIP are constant. The equiphase plane of the PIP is called the EPP in this paper. We have an orthogonal coordinate system o–xyz. The propagation direction of the incident PIP is the bisector of angle η and parallels the z axis. The direction of the EPP in the incident PIP is represented by the normal unit vector $\hat{n}_i(\cos\beta, \cos\gamma, \cos 90°)$. The x–z and y–z planes denoted by E and F, respectively, are regarded as two reference planes for the measurement. A plane surface of the object is represented by its normal vector $\hat{v}(\theta, \phi)$. The θ and ϕ are the angles between the z axis and the projections of the normal vector $\hat{v}(\theta, \phi)$ on planes E and F, respectively. The surface of the object reflects the incident PIP. The direction of the EPP in the reflected PIP is represented by its normal unit vector $\hat{n}(n_{x'}, n_y, n_{z'})$. The o'–$x'yz'$ is another orthogonal coordinate system in which the angle between the x and x' axes is 2θ. The normal vector $\hat{n}$ is determined by the normal vector unit $\hat{n}_i$ and the normal vector $\hat{v}(\theta, \phi)$.

First, let us derive the expression of $\hat{n}(n_{x'}, n_y, n_{z'})$. When $\theta = \phi = 0$ the normal unit vector $\hat{n}_0$ of the EPP in the reflected PIP is equal to the normal unit vector $\hat{n}_i$ of the EPP in the incident PIP. As shown in Fig. 2(a), $\hat{n}_0$ is given by

$$\hat{n}_0 = \{n_{0x}, n_{0y}, n_{0z}\}, \tag{1}$$

where

$$n_{0x} = \cos\beta, \qquad n_{0y} = \cos\gamma, \qquad n_{0z} = \cos 90° = 0. \tag{2}$$

When $\theta \neq 0$, angle θ of the object makes the EPP in the reflected PIP rotate by angle 2θ around the y axis. This means that vector $\mathbf{n}_{0x}$ rotates by angle 2θ around the y axis in the x–z plane and vector $\mathbf{n}_{0y}$ does not change, as shown in Fig. 2(b). The normal unit

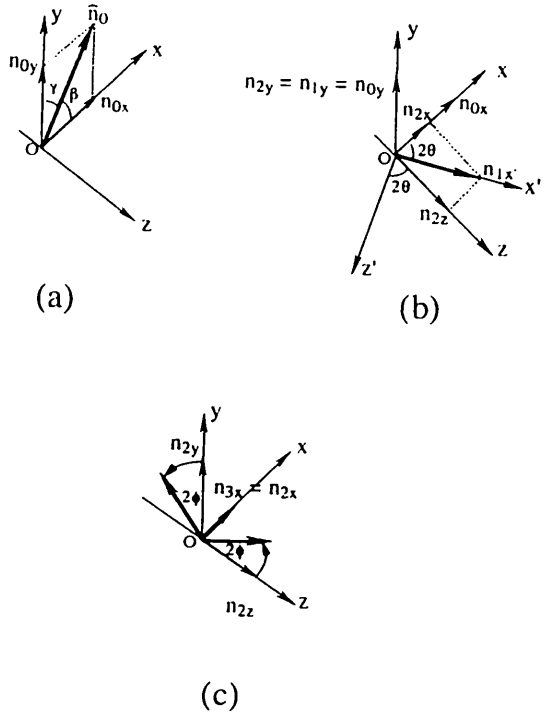

Fig. 2. Change in the unit normal vector $\hat{n}$ of the reflected equiphase plane. (a) Unit normal vector $\hat{n}_0$ at $\theta = \phi = 0$. (b) Rotation of vector $\hat{n}_0$ by angle θ of the object. (c) Rotation of vector $\hat{n}_2$ by angle ϕ of the object.

vector $\hat{n}_0$ changes to

$$\hat{n}_1 = \{n_{1x'}, n_{1y}, n_{1z'}\}, \tag{3}$$

where

$$n_{1x'} = \cos\beta, \qquad n_{1y} = \cos\gamma, \qquad n_{1z'} = 0. \tag{4}$$

In the coordinate system o–xyz, $\hat{n}_1$ is expressed as

$$\hat{n}_2 = \{n_{2x}, n_{2y}, n_{2z}\}, \tag{5}$$

where

$$n_{2x} = n_{1x'}\cos 2\theta, \qquad n_{2y} = n_{1y}, \qquad n_{2z} = n_{1x'}\sin 2\theta. \tag{6}$$

When $\phi \neq 0$, angle ϕ of the object makes the EPP in the reflected pattern rotate by angle 2ϕ around the x axis. This means that vectors $\mathbf{n}_{2y}$ and $\mathbf{n}_{2z}$ rotate by angle 2ϕ around the x axis in the y–z plane and the vector $\mathbf{n}_{2x}$ does not change, as shown in Fig. 2(c). Thus the normal unit vector $\hat{n}_2$ changes to

$$\hat{n}_3 = \{n_{3x}, n_{3y}, n_{3z}\}, \tag{7}$$

where

$$n_{3x} = n_{2x}, \qquad n_{3y} = n_{1y}\cos 2\phi + n_{2z}\sin 2\phi,$$
$$n_{3z} = -n_{1y}\sin 2\phi + n_{2z}\cos 2\phi. \tag{8}$$

Substituting Eqs. (4) and (6) into Eqs. (8), we have

$$n_{3x} = \cos\beta\cos 2\theta,$$
$$n_{3y} = \cos\gamma\cos 2\phi + \cos\beta\sin 2\theta\sin 2\phi,$$
$$n_{3z} = -\cos\gamma\sin 2\phi + \cos\beta\cos 2\phi\sin 2\theta. \tag{9}$$

Making a coordinate transformation from the o–xyz system to the o'–$x'yz'$ system for the expression of $\hat{n}_3$, we obtain the expression of the normal unit vector $\hat{n}$ in the o'–$x'yz'$ system as follows:

$$\hat{n} = \{n_{x'}, n_y, n_{z'}\}, \tag{10}$$

where

$$n_{x'} = n_{3x} \cos 2\theta + n_{3z} \sin 2\theta, \qquad n_y = n_{3y},$$

$$n_{z'} = -n_{3x} \sin 2\theta + n_{3z} \cos 2\theta. \tag{11}$$

The two points, A(0, 0, 0) and B(x_0', y_0, $-z_0'$), in the o'–$x'yz'$ system are used to detect the phases of the reflected PIP. The distance between the two EPP's that contain points A and B, respectively, is denoted by d_0. By defining vector **AB** that connects points A and B, we have

$$d_0(\beta, \gamma, \theta, \phi) = \mathbf{n} \cdot \mathbf{AB} = n_x x_0' + n_y y_0 - n_z z_0'. \tag{12}$$

The phase difference between the two EPP's is expressed as $\alpha_0 = |\alpha_A - \alpha_B|$ where α_A and α_B are the phases detected at the A and B points, respectively. We obtain another expression for d_0 as

$$d_0(\beta, \gamma, \theta, \phi) = \frac{\alpha_0}{2\pi} S, \tag{13}$$

where S is the period of the parallel interference pattern. S is given by

$$S = \frac{\lambda}{2 \sin(\eta/2)}, \tag{14}$$

where λ is the wavelength of the laser.

A small rotation of the surface in two dimensions causes the normal vector $\hat{v}(\theta, \phi)$ to change to $\hat{v}(\theta + \Delta\theta, \phi + \Delta\phi)$. The $\Delta\theta$ and $\Delta\phi$ are 2D small rotation angles of the object around the x and the y axes, respectively. Substituting $\theta + \Delta\theta$ and $\phi + \Delta\phi$ for θ and ϕ, respectively, in Eq. (9) and performing the coordinate transformation given by Eq. (11), we obtain the expression of the normal unit vector $\hat{n}$ in the o'–$x'yz'$ system after the 2D small rotation of the object. This expression is given by Eq. (A1). The distance between the two EPP's containing A and B points, respectively, after the 2D small rotation is written as

$$d(\beta, \gamma, \theta, \phi, \Delta\theta, \Delta\phi) = \mathbf{n} \cdot \mathbf{AB}. \tag{15}$$

The phase difference α detected at A and B is expressed as $\alpha = |\alpha_a - \alpha_b|$, where α_a and α_b are the phases detected at A and B, respectively, after the 2D small rotation of the object. We obtain another expression for d as

$$d(\beta, \gamma, \theta, \phi, \Delta\theta, \Delta\phi) = \frac{\alpha}{2\pi} S. \tag{16}$$

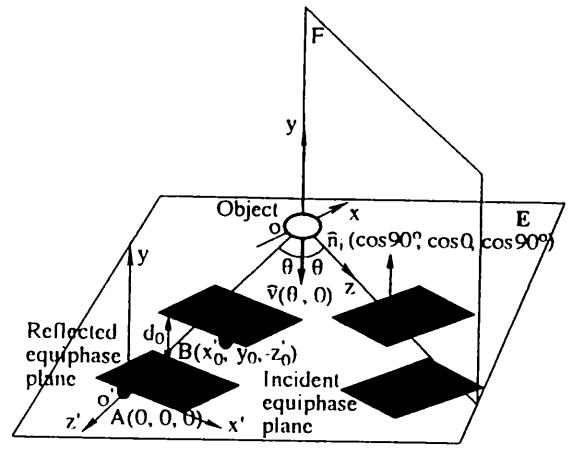

Fig. 3. Ideal configuration for measuring small rotation angle $\Delta\phi$.

From Eqs. (13) and (16), we have

$$d(\beta, \gamma, \theta, \phi, \Delta\theta, \Delta\phi) - d_0(\beta, \gamma, \theta, \phi) = \frac{\Delta\alpha}{2\pi} S, \tag{17}$$

where

$$\Delta\alpha = \alpha - \alpha_0. \tag{18}$$

Equation (17) shows the relationship of $\Delta\alpha$, $\Delta\theta$, and $\Delta\phi$. Parameters β, γ, θ, ϕ are related to the measurement configuration. If we select appropriate values for the parameters, the value of $\Delta\theta$ or $\Delta\phi$ can be obtained from $\Delta\alpha$. In Section 3 we discuss these appropriate values.

3. Configurations for the Measurement of 2D Rotation Angles

We are interested in how to measure $\Delta\phi$ or $\Delta\theta$ independently. As shown in Fig. 3, when $\phi = 0$ and the EPP's in the incident PIP parallel plane E, that is, $\beta = 90°$ and $\gamma = 0$, by using the approximations for a trigonometric function such as $\sin 2\Delta\theta \cong 2\Delta\theta$, $\sin 2\Delta\phi \cong 2\Delta\phi$, $\cos 2\Delta\theta \cong 1$, $\cos 2\Delta\phi \cong 1$ in Eqs. (12) and (15), respectively, we have

$$d_0 = y_0, \tag{19}$$

$$d = y_0 + 2\Delta\phi(z_0' \cos 2\theta - x_0' \sin 2\theta). \tag{20}$$

Equations (19) and (20) are also found in Eqs. (A4) and (A5) in the conditions of $\phi = 0$ and $\delta_1 = 0$. From Eqs. (19) and (20), $\Delta\phi$ is given by

$$\Delta\phi = \frac{d - d_0}{2z_0''}, \tag{21}$$

where

$$z_0'' = (z_0' \cos 2\theta - x_0' \sin 2\theta). \tag{22}$$

Substituting Eq. (17) into Eq. (21), we express $\Delta\phi$ as

$$\Delta\phi = \frac{\Delta\alpha}{4\pi z_0''} S. \tag{23}$$

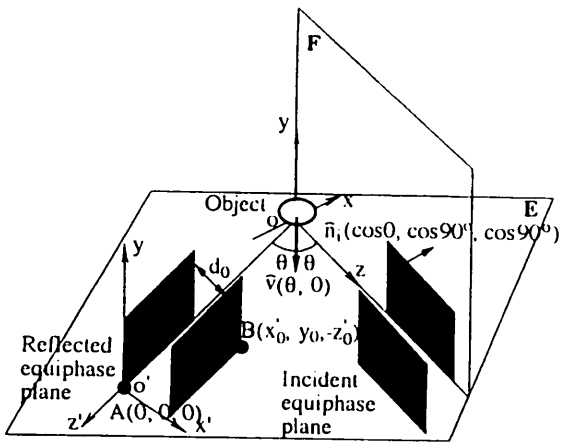

Fig. 4. Ideal configuration for measuring small rotation angle $\Delta\theta$.

It is clear that the measurement configuration of Fig. 3 provides an independent measurement of $\Delta\phi$ without any effect from $\Delta\theta$. It is obvious that we can independently measure $\Delta\theta$ without any effect from $\Delta\phi$ by using the measurement configuration where the EPP in the incident PIP parallels the F plane and $\theta = 0$, $\phi \neq 0$ in vector $\hat{v}(\theta, \phi)$. However, the two measurement configurations cannot be combined because vector $\hat{v}(\theta, \phi)$ is different in the two configurations. To measure simultaneously the 2D small rotation angles, $\Delta\phi$ and $\Delta\theta$, we construct the configuration for measuring $\Delta\theta$ shown in Fig. 4 with the same phase-detecting points as those in Fig. 3. In the configuration the EPP's in the incident PIP parallel plane F, that is, $\beta = 0$ and $\gamma = 90°$. In the same way that we obtain Eqs. (19) and (20), we have

$$d_0 = x_0', \tag{24}$$

$$d = x_0' - 2z_0'\Delta\theta + 2y_0\Delta\phi \sin 2\theta. \tag{25}$$

Equations (24) and (25) are also found in Eqs. (A7) in the conditions of $\phi = 0$, $\delta_2 = 0$. Substituting Eqs. (24) into (25), we have

$$\Delta\theta = -\frac{d - d_0}{2z_0'} + \varphi, \tag{26}$$

where

$$\varphi = (y_0\Delta\phi \sin 2\theta)/z_0'. \tag{27}$$

When $z_0' \gg y_0$ and θ are small, φ is small enough to be neglected in Eq. (27). For example, when $z_0' = 120$ mm, $y_0 = 1$ mm, $\theta = 5°$, and $\Delta\phi = 60$ arcsec, we have $\varphi = 0.087$ arcsec. Substituting Eq. (17) into Eq. (26) and neglecting φ, we give the expression of $\Delta\theta$ by

$$\Delta\theta = -\frac{\Delta\alpha}{4\pi z_0'} S. \tag{28}$$

Therefore we combine the two measurement configurations in Figs. 3 and 4. Two kinds of $\Delta\alpha$s of the reflected orthogonal PIP's are detected, and the 2D small rotation angles are simultaneously measured by Eqs. (23) and (28).

4. Nonideal Measurement Configurations

We refer to the measurement configuration in Fig. 3 or 4 as an ideal measurement configuration in which the EPP in the incident PIP is absolutely parallel to plane E or F and $\phi = 0$ in vector $\hat{v}(\theta, \phi)$. But in practice measurements, it is difficult to obtain absolute alignments of the EPP's and the object. Now angle ϕ is not zero. The normal unit vector $\hat{n}_i$ of the EPP in the incident PIP in Fig. 1 is expressed as

$$\beta = 90° - \delta_1, \qquad \gamma = \delta_1, \tag{29}$$

where angle δ_1 is the inclination angle of the EPP in Fig. 3. Similarly, the normal unit vector $\hat{n}_i$ of the EPP in the incident PIP in Fig. 1 is expressed as

$$\beta = \delta_2, \qquad \gamma = 90° - \delta_2, \tag{30}$$

where angle δ_2 is the inclination angle of the EPP in Fig. 4. We refer to these measurement configurations as nonideal measurement configurations. In the nonideal measurement configurations, we measure two kinds of $\Delta\alpha$s and obtain the 2D rotation angles from Eqs. (23) and (28). These measured rotation angles are denoted by $\Delta\phi_m$ and $\Delta\theta_m$. Derivations of $\Delta\phi_m$ and $\Delta\theta_m$ are given in Appendix A. They are expressed as follows:

$$\Delta\phi_m = -R_{11}\Delta\theta + R_{12}\Delta\phi, \tag{31}$$

$$\Delta\theta_m = R_{21}\Delta\theta - R_{22}\Delta\phi, \tag{32}$$

where

$$R_{11} = \sin\delta_1\left[\frac{z_0'}{z_0''} - 2\cos 2\theta \sin\phi\left(\sin\phi + \frac{y_0}{z_0''}\cos\phi\right)\right], \tag{33}$$

$$R_{12} = \sin\delta_1 \sin 2\theta\left(\sin 2\phi + \frac{y_0}{z_0''}\cos 2\phi\right) + \cos\delta_1\left(\cos 2\phi - \frac{y_0}{z_0''}\sin 2\phi\right), \tag{34}$$

$$R_{21} = \cos\delta_2\left[1 - 2\cos 2\theta \sin\phi\left(\frac{z_0''}{z_0'}\sin\phi + \frac{y_0}{z_0'}\cos\phi\right)\right], \tag{35}$$

$$R_{22} = \left[\cos\delta_2 \sin 2\theta\left(\frac{z_0''}{z_0'}\sin 2\phi + \frac{y_0}{z_0'}\cos 2\phi\right) + \sin\delta_2\left(\frac{z_0''}{z_0'}\cos 2\phi - \frac{y_0}{z_0'}\sin 2\phi\right)\right]. \tag{36}$$

If we know the values of R_{11}, R_{12}, R_{21}, and R_{22}, we can obtain the actual angles $\Delta\phi$ and $\Delta\theta$ from the measured values $\Delta\phi_m$ and $\Delta\theta_m$ by solving Eqs. (31) and (32). Coefficients R_{11}, R_{12}, R_{21}, and R_{22} contain the values of δ_1, δ_2, θ, ϕ, x_0', y_0, and z_0'. It is im-

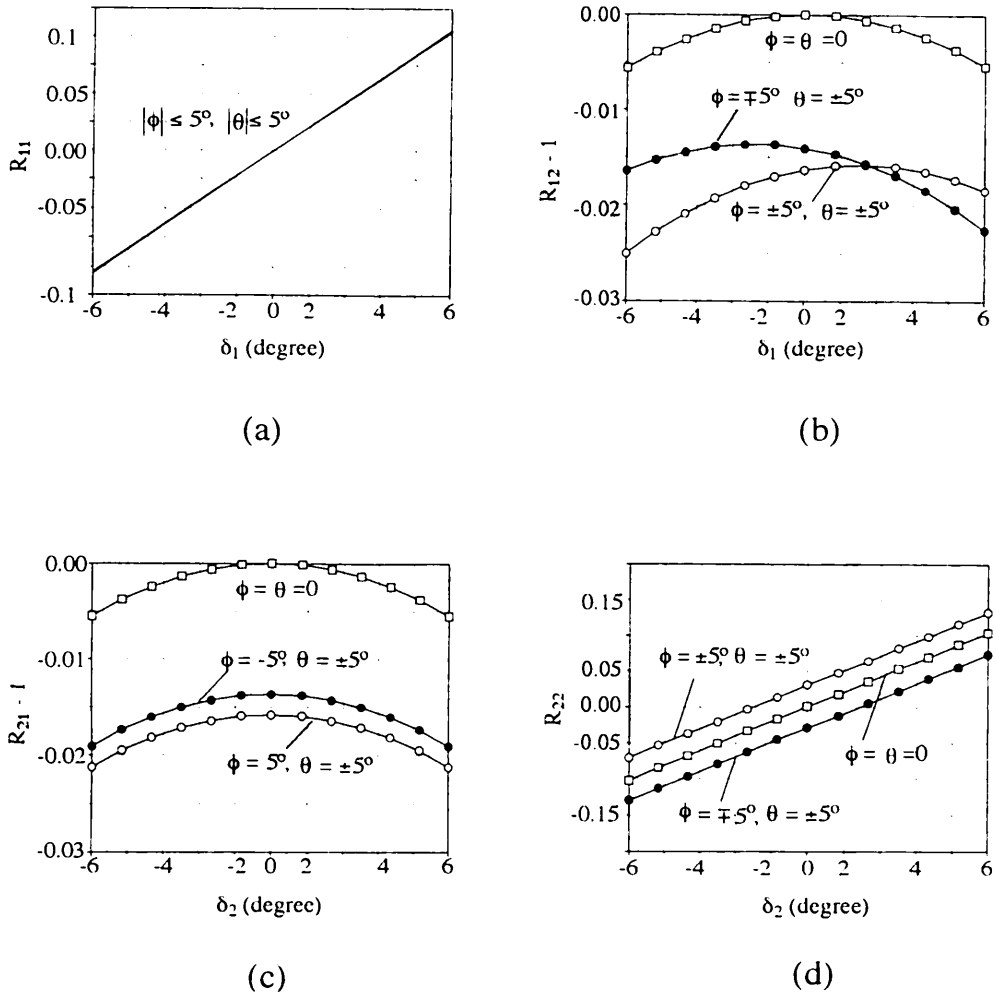

Fig. 5. Relationships of ratios R_{11}, R_{12}, R_{21}, R_{22} and angles δ_1, δ_2, θ, ϕ. (a) Ratio R_{11} versus angles δ_1, θ, ϕ. (b) Ratio R_{12} versus angles δ_1, θ, ϕ. (c) Ratio R_{21} versus angles δ_2, θ, ϕ. (d) Ratio R_{22} versus angles δ_2, θ, ϕ.

possible to know the values of δ_1 and δ_2 exactly. Thus it is difficult to obtain the exact values of R_{11}, R_{12}, R_{21}, and R_{22}. However, if angles δ_1, δ_2, θ, and ϕ are within $\pm 5°$, the differences between the measured rotation angles and the actual ones are less than 10%.

$\Delta\phi_m$ and $\Delta\theta_m$ are expressed as

$$\Delta\phi_m = \Delta\phi + \varepsilon_1, \tag{37}$$

$$\Delta\theta_m = \Delta\theta + \varepsilon_2, \tag{38}$$

where

$$\varepsilon_1 = (R_{12} - 1)\Delta\phi - R_{11}\Delta\theta, \tag{39}$$

$$\varepsilon_2 = (R_{21} - 1)\Delta\theta - R_{22}\Delta\phi. \tag{40}$$

The ε_1 and ε_2 terms are regarded as errors caused by nonideal measurement configurations.

Figure 5 shows coefficients R_{11}, $R_{12} - 1$, $R_{21} - 1$, and R_{22} versus angles δ_1 and δ_2 for various values of θ and ϕ at $x_0' = y_0 = 1$ mm, and $z_0' = 120$ mm. Angles θ and ϕ are within $\pm 5°$. When angles δ_1 and δ_2 approach zero, the coefficients are close to zero except for $R_{12} - 1$ at nonzero values of θ and ϕ. The maximum value of $R_{12} - 1$ is slightly further from $\delta_1 = 0$ because of the first term in Eq. (34). The values of $R_{12} - 1$ and $R_{21} - 1$ are within -0.017 when angles δ_1 and δ_2 are within $\pm 1°$. The value of R_{11} is almost constant for the change in θ, ϕ because the second term in Eq. (33) is very small. R_{11} is within ± 0.012 when δ_1 is within $\pm 1°$. R_{22} depends on the values of θ and ϕ. R_{22} is within ± 0.04 when δ_2 is within $\pm 1°$. $R_{12} - 1$, $R_{21} - 1$, and R_{22} at $\phi = 1°$, $\theta = 5°$ are very close to their values at $\phi = 0°$, $\theta = 0°$ but are very different from them at $\phi = 5°$, $\theta = 5°$. This indicates that $R_{12} - 1$, $R_{21} - 1$, and R_{22} are more sensitive to ϕ than θ.

5. Characteristics of the Method

First, we discuss the angular sensitivity that is defined as the ratio of $\Delta\alpha$ to $\Delta\phi$ or $\Delta\theta$. From Eq. (23) the sensitivity of $\Delta\phi$ is written as

$$S_{\phi 1} = 4\pi z_0''/S_1, \tag{41}$$

where S_1 is the period space of PIP 1, which is used to measure angle $\Delta\phi$. From Eq. (28) we have the

sensitivity of $-\Delta\theta$:

$$S_{\theta 2} = 4\pi z_0'/S_2, \tag{42}$$

where S_2 is the period space of PIP 2, which is used to measure angle $\Delta\theta$. When $S_1 = S_2 = 1.5$ mm, $z_0' = 120$ mm, and $z_0'' = 118$ mm, a high angular sensitivity of ~4.9 mrad/arcsec is obtained from Eqs. (41) and (42) for the measurement of $\Delta\phi$ or $\Delta\theta$.

Second, we consider the measurement ranges. Phase difference α in Eq. (18) changes from 0 to 2π. When phase difference α_0 is equal to π in Eq. (18), from Eqs. (23) and (28) we obtain the same measurement range for the positive and negative small rotation angles:

$$|\Delta\phi| \le \frac{1}{4|z_0''|} S_1, \tag{43}$$

$$|\Delta\theta| \le \frac{1}{4|z_0'|} S_2. \tag{44}$$

When $S_1 = S_2 = 1.5$ mm, $z_0' = 120$ mm, $z_0'' = 118$ mm, the measurement range of ± 10 arcmin for $\Delta\phi$ or $\Delta\theta$ is obtained from Eqs. (43) and (44).

Third, let us consider the spatial resolution of the method. Because PIP 1 and PIP 2 are orthogonal to each other, the spatial resolution of the method is given as

$$SR = S_1 \times S_2. \tag{45}$$

When $S_1 = S_2 = 1.5$ mm, a spatial resolution of 1.5×1.5 mm^2 is obtained.

Fourth, in the practice measurement, the mechanical vibrations cause the random errors in the phase detection. Standard deviations of phase differences α_0 and α in the measurement of angle $\Delta\phi$ are donated by $\sigma_{\alpha_0}(\Delta\phi)$ and $\sigma_\alpha(\Delta\phi)$, respectively. The standard deviations in the measurement of angle $\Delta\theta$ are $\sigma_{\alpha_0}(\Delta\theta)$ and $\sigma_\alpha(\Delta\theta)$. We assume that

$$\sigma_{\alpha_0}(\Delta\phi) = \sigma_\alpha(\Delta\phi) = \sigma_{\alpha_0}(\Delta\theta) = \sigma_\alpha(\Delta\theta) = \sigma. \tag{46}$$

The random errors in the measurements of angles $\Delta\phi$ and $\Delta\theta$ are expressed by $\varepsilon_{\Delta\phi}$ and $\varepsilon_{\Delta\theta}$, respectively. From Eqs. (23) and (28) the standard deviations $\sigma_{\Delta\phi}$ and $\sigma_{\Delta\theta}$ of the random errors in the measurement of angles $\Delta\phi$ and $\Delta\theta$, respectively, are given by

$$\sigma_{\Delta\phi} = \frac{\sqrt{2}\sigma}{4\pi z_0''} S, \tag{47}$$

$$\sigma_{\Delta\theta} = \frac{\sqrt{2}\sigma}{4\pi z_0'} S. \tag{48}$$

When the feedback control systems are used to eliminate mechanical vibrations, σ decreases greatly.[7] In experiments, σ decreases to ~2 mrad from 0.1 rad by feedback controllers. From Eqs. (47) and (48), $\sigma_{\Delta\phi}$ and $\sigma_{\Delta\theta}$ are ~0.58 arcsec. Summing up the errors caused from the nonideal measurement configurations and the phase detections, we have

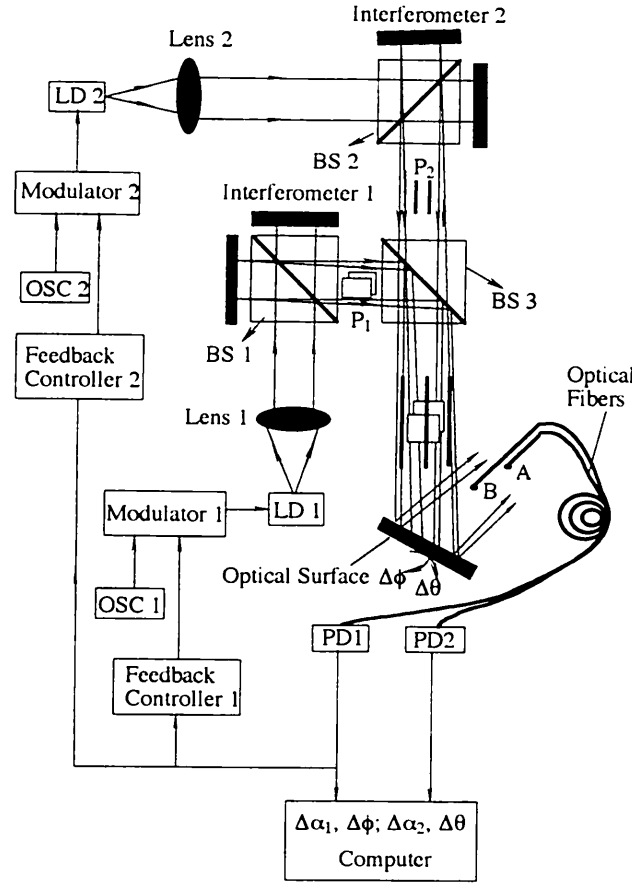

Fig. 6. Experimental setup.

$$E_{\Delta\phi} = \varepsilon_1 + \varepsilon_{\Delta\phi}, \tag{49}$$

$$E_{\Delta\theta} = \varepsilon_2 + \varepsilon_{\Delta\theta}. \tag{50}$$

$E_{\Delta\phi}$ and $E_{\Delta\theta}$ are errors in the measurement of 2D small rotation angles $\Delta\phi$ and $\Delta\theta$, respectively, and show us how accurately we can measure 2D small rotation angles $\Delta\phi$ and $\Delta\theta$ by Eqs. (23) and (28).

6. Experimental Setup

Figure 6 shows an experimental setup for measuring 2D small rotation angles $\Delta\phi$ and $\Delta\theta$. The object is an optical surface. Two Twyman–Green-type interferometers are used to generate two sets of PIP's that are orthogonal to each other. The wavelength of LD_i is 780 nm ($i = 1, 2$). The PIP P_1 from Interferometer 1 is parallel to the plane of the figure. The plane of the figure is plane E. PIP P_2 from Interferometer 2 is perpendicular to the plane of the figure. The angle between the two laser beams from interferometer i is η_i and the period of PIP P_i is S_i, respectively. The beam splitter, BS 3, is used to make patterns P_1 and P_2 overlap. They are incident on the optical surface whose normal vector has small angles θ and ϕ of less than 5°.

If we remove the optical surface, the two beams from BS 1 or BS 2 separate at a position far from the

optical surface and are observed as two spots on a plane perpendicular to plane E. The distance between the centers of the two spots from BS 1 indicates the value of angle η_1, and the distance between the centers of two spots along a line parallel to plane E indicates a value of misalignment angle δ_1 for PIP P_1. In the same way we know the value of angle η_2 and the value of the misalignment angle δ_2 for PIP P_2. By the positions of two pairs spots, we adjust angles η_1, η_2, δ_1, δ_2.

Because distance d_0 between the two detection points, A and B, is less than space S, two fibers stuck together are used to detect the interference signals at the two points. The outsider diameters of the fibers are ~1 mm, and their core diameters are 50 μm. The optical fibers are placed parallel to plane E and along the propagation direction of reflected laser beams to receive the light at points A and B. Thus the direction of the optical fibers is along the z' axis as shown in Fig. 3. The value of angle θ is determined by the angle between the optical fibers and the propagation direction of the incident PIP. The value of angle θ is determined. The distance between points A and B along the optical fibers corresponds to the value of z_0', and the distance between two optical fibers along axes x' and y corresponds to the values of x_0' and y_0, respectively. In our experiment the parameters are $x_0' = y_0 = 0.75$ mm, $z_0' = 120$ mm, $z_0'' = 118$ mm, and $\theta = 5°$.

Two sinusoidal phase-modulating laser-diode interferometers are used. To distinguish the interference signals from Interferometers 1 and 2, the injection currents of two laser diodes are modulated with the sinusoidal wave signals of $z_1 \cos \omega_1 t$ and $z_2 \cos \omega_2 t$, respectively.[8] In our experiment, $\omega_1/2\pi$ and $\omega_2/2\pi$ are 8 and 1 kHz, respectively. The two interference signals detected at points A and B are expressed as

$$S_A = S_{1A}[\cos(z_1 \cos \omega_1 t + \alpha_{1A})] + S_{2A}[\cos(z_2 \cos \omega_2 t + \alpha_{2A})], \quad (51)$$

$$S_B = S_{1B}[\cos(z_1 \cos \omega_1 t + \alpha_{1B})] + S_{2B}[\cos(z_2 \cos \omega_2 t + \alpha_{2B})]. \quad (52)$$

The two optical fibers are connected with two photodiodes, PD1 and PD2. Interference signals S_A and S_B are sent into a computer through an analog-to-digital converter. With the technique of sinusoidal phase-modulating interferometry the values of phases α_{iA}, α_{iB} ($i = 1, 2$) are detected. Thus we obtain two kinds of phase difference $\alpha_0 s$ for PIP P_1 and PIP P_2. After the object rotates in two dimensions in the same way we also obtain two kinds of phase difference αs for PIP P_1 and PIP P_2. Therefore 2D small rotation angles $\Delta\phi$ and $\Delta\theta$ are measured by Eqs. (23) and (28). Feedback Controllers 1 and 2 are used in Interferometers 1 and 2, respectively, to eliminate mechanical vibrations.

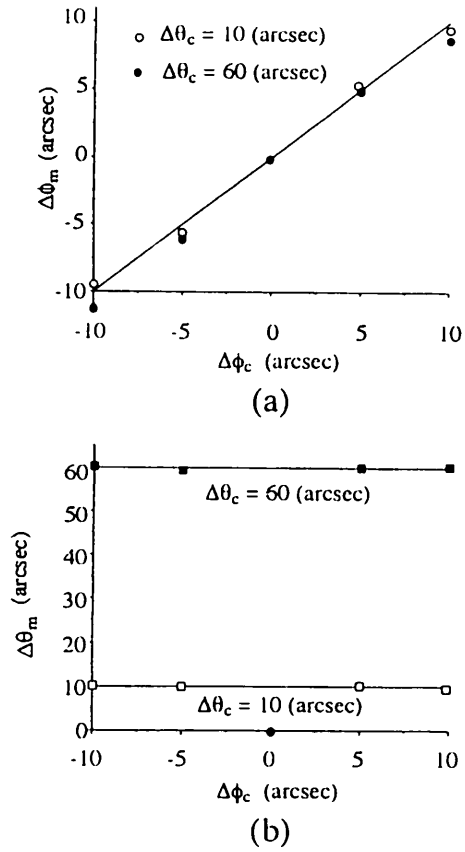

Fig. 7. Measurement results of errors $E_{\Delta\phi}$ and $E_{\Delta\theta}$ at $\Delta\theta_c = 10$ and 60 arcsec, respectively.

7. Experimental Results

Experiments were performed with the experimental setup in Fig. 6. In the experiments the related parameters were $S_1 = S_2 = 1.5$ mm, $x_0' = y_0 = 750$ μm, $z_0' = 120$ mm, and $z_0'' = 118$ mm at $\phi = 1°$ and $\theta = 5°$. The 2D small rotation angles, $\Delta\phi$ and $\Delta\theta$, were measured by our method and with an autocollimator. The results with our method are expressed as $\Delta\phi_m$ and $\Delta\theta_m$. The results with the autocollimator are expressed as $\Delta\phi_c$ and $\Delta\theta_c$. The values of $\Delta\phi_m - \Delta\phi_c$ and $\Delta\theta_m - \Delta\theta_c$ correspond to errors $E_{\Delta\phi}$ and $E_{\Delta\theta}$, respectively. The initial position of the object is indicated by the black dot at $\Delta\phi_c = 0$, $\Delta\theta_c = 0$, $\Delta\phi_m = 0$, and $\Delta\theta_c = 0$ in Figs. 7–10.

A. Measurement Errors

Measurement errors $E_{\Delta\phi}$ and $E_{\Delta\theta}$ are given theoretically by Eqs. (49) and (50). Random errors $\varepsilon_{\Delta\phi}$ and $\varepsilon_{\Delta\theta}$ are estimated to be within ±0.6 arcsec. Errors ε_1 and ε_2 are given by Eqs. (39) and (40). We investigate how the errors in the measurement appear and if the experimental results agree with the theoretical results. Figure 7(a) shows that rotation angle $\Delta\phi$ within ±10 arcsec was measured at intervals of 5 arcsec in the conditions of $\Delta\theta_c = 10$ and 60 arcsec. When $\Delta\theta_c = 10$ arcsec, error $E_{\Delta\phi}$ was random and within ±0.6 arcsec. This is due to random error $\varepsilon_{\Delta\phi}$. When $\Delta\theta_c = 60$ arcsec, error $E_{\Delta\phi}$ was from −1.3 to

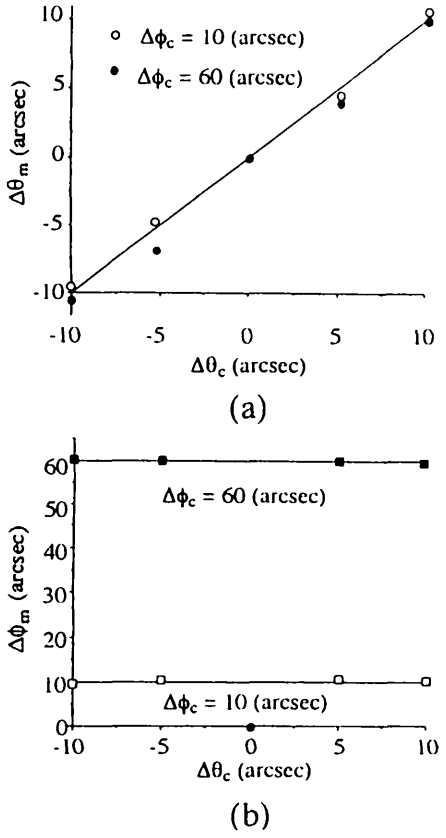

Fig. 8. Measurement results of errors $E_{\Delta\theta}$ and $E_{\Delta\phi}$ at $\Delta\phi_c$ = 10 and 60 arcsec, respectively.

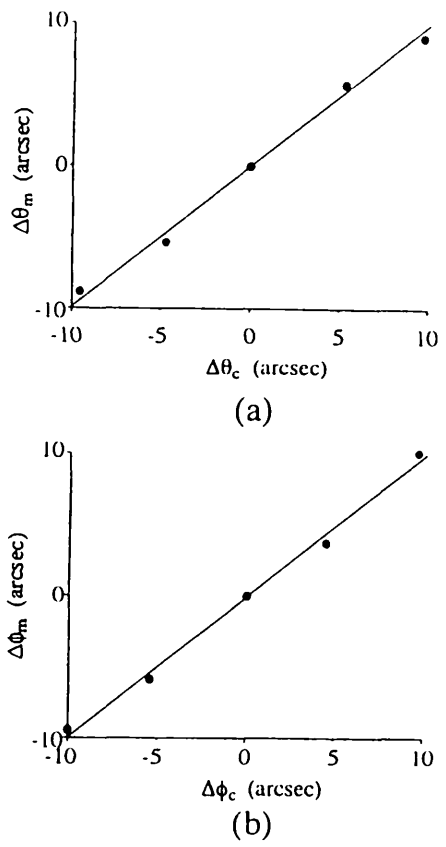

Fig. 9. Measurement results of 2D small rotation angles $\Delta\phi$, $\Delta\theta$ within ±10 arcsec.

−0.1 arcsec. This error has a minus bias of −0.7, which is due to the large value of $\Delta\theta$. This error is considered to be ε_1. From Eq. (39) the value of R_{11} is positive and estimated to be ~0.01. So the value of δ_1 is estimated to be ~1° from Fig. 5(a). In Fig. 5 the curves at ϕ = 0°, θ = 0° are used when we estimate the values of δ_1 and δ_2 in conditions ϕ = 1°, θ = 5°. Rotation angle $\Delta\theta$ was simultaneously measured for $\Delta\theta_c$ = 10 and 60 arcsec as shown in Fig. 7(b). At $\Delta\theta_c$ = 10 arcsec, error $E_{\Delta\theta}$ was random and within ±0.6 arcsec. This is from random error $\varepsilon_{\Delta\theta}$. At $\Delta\theta_c$ = 60 arcsec, error $E_{\Delta\theta}$ was still random and almost within ±0.6 arcsec. Error $E_{\Delta\theta}$ has no effect on $\Delta\theta$. From Eq. (40) the value of R_{21} − 1 is estimated to be almost zero. We estimate from Fig. 5(c) that the value of δ_2 is within ±1°.

As shown in Fig. 8(a) the small rotation angle $\Delta\theta$ within ±10 arcsec was measured at intervals of 5 arcsec in conditions of $\Delta\phi_c$ = 10 and 60 arcsec. When $\Delta\phi_c$ = 10 arcsec, error $E_{\Delta\theta}$ in the measurement was from random error $\varepsilon_{\Delta\phi}$. When $\Delta\phi_c$ = 60 arcsec, error $E_{\Delta\theta}$ was from −1.5 to −0.2 arcsec. The minus bias of −0.85 in the error is caused from the large value of $\Delta\phi$. This error is considered to be ε_2. From Eq. (40) R_{22} is positive and estimated to be ~0.01. So we estimate from Fig. 5(d) that the value of δ_2 is ~1°. This value of δ_2 agrees with the results from the value of R_{21} − 1. Figure 8(b) shows that the small rotation angle $\Delta\phi$ was simultaneously measured by our method for $\Delta\phi_c$ = 10 and 60 arcsec. When $\Delta\phi_c$ = 10 arcsec, error $E_{\Delta\phi}$ was random and within ±0.6 arcsec. This is due to random error $\varepsilon_{\Delta\phi}$. When $\Delta\phi_c$ = 60 arcsec, error $E_{\Delta\phi}$ was still random and almost within ±0.6 arcsec. It is clear that the large value of $\Delta\phi$ does not affect error $E_{\Delta\phi}$. We estimate from Eq. (39) that the value of R_{12} − 1 is almost zero and from Fig. 5(b) that the value of δ_1 is from −1° to 1°. This value of δ_1 agrees with the result from the values of R_{11}.

From these experimental results we obtain the values of δ_1 and δ_2 by using the results of our theoretical

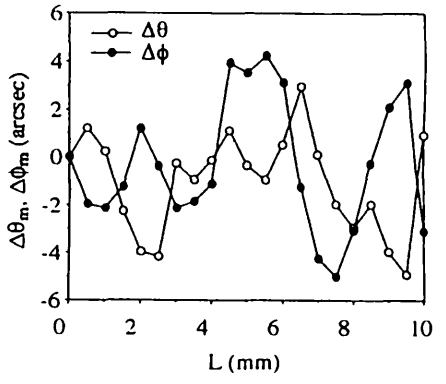

Fig. 10. Measurement results of 2D small rotation angles from displacements of a stage.

analysis. It is shown that δ_1 and δ_2 can be adjusted to be less than 1°, and the theoretical analysis is supported by the experimental results. The configurations of the setup were $\phi = 1°$, $\theta = 5°$, and $\delta_1 = \delta_2 \approx 1°$, and we have $R_{12} - 1 \approx R_{21} - 1 \approx 0$ and $R_{11} \approx R_{22} \approx 0.01$ in Eqs. (39) and (40). Then error ε_1 in the measurement of $\Delta\phi$ is almost equal to $-0.01\Delta\theta$, and error ε_2 in the measurement of $\Delta\theta$ is almost equal to $-0.01\Delta\phi$. Therefore random errors $\varepsilon_{\Delta\phi}$ and $\varepsilon_{\Delta\theta}$ are dominant when values of $\Delta\phi$ and $\Delta\theta$ are within ± 10 arcsec. When $\Delta\phi$ and $\Delta\theta$ are large, ε_1 and ε_2 produce bias values in the measurement.

B. Measurement of 2D Small Rotation Angles

We gave the 2D small rotation angles, $\Delta\phi$ and $\Delta\theta$, at intervals of ~5 arcsec within ± 10 arcsec. The measurement results are shown in Fig. 9. We can see that measurement errors $E_{\Delta\phi}$ and $E_{\Delta\theta}$ are within ± 0.6 arcsec, and the errors caused from ε_1 and ε_2 are almost zero. The measurement range of the 2D small rotation angles was almost from -10 to 10 arcmin, which is expected from Eqs. (43) and (44). In this range the maximum values of errors $E_{\Delta\phi}$ and $E_{\Delta\theta}$ were ± 0.1 arcmin, which are from errors ε_1 and ε_2. The results agree with the conclusions in Subsection 7.A.

When a stage with a mirror is moved by a micrometer, displacement makes the stage rotate. It is important to investigate how the stage rotates through displacements. We applied our method to measuring 2D small rotation angles of the mirror attached to the stage. An axis of the rotation angle, $\Delta\theta$, to be measured was perpendicular to the surface of the stage. Another axis of the rotation angle, $\Delta\phi$, was perpendicular both to the axis of the rotation angle, $\Delta\theta$, and to the direction of the displacement. The measurement results are shown in Fig. 10. In the measurement, the stage was moved at intervals of 0.5 mm in a range of 10 mm, and rotations of the mirror were measured at each interval. The results show that the displacement makes the stage rotate around the two axes between 4.7 and -5.2 arcsec in two dimensions.

8. Conclusions

A method of measuring a one-dimensional small rotation angle with a PIP has been developed for measuring 2D small rotation angles. By analyzing the PIP reflected by an optical surface, we obtained the phase difference α of the reflected PIP between the two phase detection points A and B. From the relationships between phase difference α and the 2D small rotation angles of $\Delta\theta$ and $\Delta\phi$, we determined two kinds of PIP to measure simultaneously the 2D small rotation angles. We analyzed errors ε_1 and ε_2 caused in the nonideal configuration where the required alignments between the two PIP's and the object are not satisfied. By using a feedback control system in sinusoidal phase-modulating interferometry, we reduced random errors $\varepsilon_{\Delta\phi}$ and $\varepsilon_{\Delta\theta}$ caused by mechanical vibration. In experiments the measurement errors were investigated in detail. It was found from the experimental results and the theoretical analysis that the inclination angles of the two PIP's were adjusted to be ~1°. We reached the following conclusions: (1) Error ε_1 in the measurement of $\Delta\phi$ is almost equal to $-0.01\Delta\theta$, and error ε_2 in the measurement of $\Delta\theta$ is almost equal to $-0.01\Delta\phi$. (2) For small rotation angles of less than a few tens of arcseconds, random errors $\varepsilon_{\Delta\phi}$ and $\varepsilon_{\Delta\theta}$ whose standard deviations are 0.6 arcsec are dominant, and, for the large rotation angles, errors ε_1 and ε_2 produce bias values in the measured values. The theoretical analysis was supported by the experimental results. With the advantages of a high space resolution of 1.5×1.5 mm^2 and a high sensitivity of 4.9 mrad/arcsec, the method is suitable for measuring 2D small rotation angles of the object, which has a small surface.

Appendix A: Derivation of Eqs. (31) and (32)

We obtain an expression for the normal unit vector $\hat{n}$ in the o'–$x'yz'$ system:

$$\begin{aligned} n_{x'} &= \cos\beta\cos 2(\theta + \Delta\theta)\cos 2\theta - [\cos\gamma\sin 2(\phi + \Delta\phi) \\ &\quad - \cos\beta\cos 2(\phi + \Delta\phi)\sin 2(\theta + \Delta\theta)]\sin 2\theta, \\ n_y &= \cos\gamma\cos 2(\phi + \Delta\phi) + \cos\beta\sin 2(\phi + \Delta\phi) \\ &\quad \times \sin 2(\theta + \Delta\theta), \\ n_{z'} &= -\cos\beta\cos 2(\theta + \Delta\theta)\sin 2\theta - [\cos\gamma\sin 2 \\ &\quad \times (\phi + \Delta\phi) - \cos\beta\cos 2(\phi + \Delta\phi)\sin 2 \\ &\quad \times (\theta + \Delta\theta)]\cos 2\theta. \end{aligned} \tag{A1}$$

On substituting $\beta = 90° - \delta_1$, $\gamma = \delta_1$ into Eq. (A1), we obtain

$$\begin{aligned} n_{x'} &= \sin\delta_1\cos 2(\theta + \Delta\theta)\cos 2\theta \\ &\quad - [\cos\delta_1\sin 2(\phi + \Delta\phi) - \sin\delta_1\cos 2(\phi + \Delta\phi) \\ &\quad \times \sin 2(\theta + \Delta\theta)]\sin 2\theta, \\ n_y &= \cos\delta_1\cos 2(\phi + \Delta\phi) + \sin\delta_1\sin 2(\phi + \Delta\phi) \\ &\quad \times \sin 2(\theta + \Delta\theta), \\ n_{z'} &= -\sin\delta_1\cos 2(\theta + \Delta\theta)\sin 2\theta \\ &\quad - [\cos\delta_1\sin 2(\phi + \Delta\phi) - \sin\delta_1 \\ &\quad \times \cos 2(\phi + \Delta\phi)\sin 2(\theta + \Delta\theta)]\cos 2\theta. \end{aligned} \tag{A2}$$

Using approximations for a trigonometric function such as $\sin 2\Delta\theta \cong 2\Delta\theta$, $\sin 2\Delta\phi \cong 2\Delta\phi$, $\cos 2\Delta\theta \cong 1$, $\cos 2\Delta\phi \cong 1$ and neglecting the terms that contain $\Delta\theta \times \Delta\phi$, we have

$$\begin{aligned} n_{x'} &= \sin\delta_1\cos^2 2\theta - 2\Delta\theta\sin\delta_1\sin 2\theta\cos 2\theta \\ &\quad - \cos\delta_1\sin 2\phi\sin 2\theta - 2\Delta\phi\cos\delta_1\cos 2\phi\sin 2\theta \\ &\quad + \sin\delta_1\sin 2\theta(\sin 2\theta\cos 2\phi \\ &\quad - 2\Delta\phi\sin 2\phi\sin 2\theta + 2\Delta\theta\cos 2\theta\cos 2\phi), \end{aligned} \tag{A3a}$$

$$n_y = \cos\delta_1(\cos 2\phi - 2\Delta\phi \sin 2\phi) + \sin\delta_1(\sin 2\phi \sin 2\theta + 2\Delta\phi \cos 2\phi \sin 2\theta + 2\Delta\theta \cos 2\theta \sin 2\phi),$$

$$n_z = -\sin\delta_1 \cos 2\theta \sin 2\theta + 2\Delta\theta \sin\delta_1 \sin^2 2\theta - \cos 2\theta \cos\delta_1(\sin 2\phi + 2\Delta\phi \cos 2\phi) + \cos 2\theta \sin\delta_1(\cos 2\phi \sin 2\theta - 2\Delta\phi \sin 2\phi \sin 2\theta + 2\Delta\theta \cos 2\theta \cos 2\phi). \quad \text{(A3b)}$$

Substituting Eqs. (A3) into Eq. (15) and assuming that $\Delta\theta = \Delta\phi = 0$, the expression for $d_0(\beta, \gamma, \theta, \phi)$ is written as

$$d_0(\beta, \gamma, \theta, \phi) = x_0'[\sin\delta_1(1 - 2\sin^2 2\theta \sin^2\phi) - \cos\delta_1 \sin 2\phi \sin 2\theta] + y_0(\cos\delta_1 \cos 2\phi + \sin\delta_1 \sin 2\phi \sin 2\theta) + 2z_0' \cos 2\theta \sin\phi(\sin\delta_1 \sin 2\theta \sin\phi + \cos\delta_1 \cos\phi). \quad \text{(A4)}$$

The expression of $d(\beta, \gamma, \theta, \phi, \Delta\theta, \Delta\phi) - d_0(\beta, \gamma, \theta, \phi)$ is given by

$$d(\beta, \gamma, \theta, \phi, \Delta\theta, \Delta\phi) - d_0(\beta, \gamma, \theta, \phi) = 2\Delta\theta \sin\delta_1[2 \cos 2\theta \sin\phi(z_0'' \sin\phi + y_0 \cos\phi) - z_0'] + 2\Delta\phi[\sin\delta_1 \sin 2\theta(z_0'' \sin 2\phi + y_0 \cos 2\phi) + \cos\delta_1(z_0'' \cos 2\phi - y_0 \sin 2\phi)], \quad \text{(A5)}$$

where $z_0' \cos 2\theta - x_0' \sin 2\theta = z_0''$.

Substituting Eq. (A5) into Eq. (21), we have

$$\Delta\phi_m = -\Delta\theta \sin\delta_1\left[\frac{z_0'}{z_0''} - 2\cos 2\theta \sin\phi \times \left(\sin\phi + \frac{y_0}{z_0''}\cos\phi\right)\right] + \Delta\phi\left[\sin\delta_1 \sin 2\theta\left(\sin 2\phi + \frac{y_0}{z_0''}\cos 2\phi\right) + \cos\delta_1\left(\cos 2\phi - \frac{y_0}{z_0''}\sin 2\phi\right)\right]. \quad \text{(A6)}$$

When $\beta = \delta_2$, $\gamma = 90° - \delta_2$, we replace $\sin\delta_1$ and $\cos\delta_1$ in Eq. (A5) with $\cos\delta_2$ and $\sin\delta_2$, respectively, and we have

$$d(\beta, \gamma, \theta, \phi, \Delta\theta, \Delta\phi) - d_0(\beta, \gamma, \theta, \phi) = 2\Delta\theta \cos\delta_2[2 \cos 2\theta \sin\phi(z_0'' \sin\phi + y_0 \cos\phi) - z_0'] + 2\Delta\phi[\cos\delta_2 \sin 2\theta(z_0'' \sin 2\phi + y_0 \cos 2\phi) + \sin\delta_2(z_0'' \cos 2\phi - y_0 \sin 2\phi)]. \quad \text{(A7)}$$

On substituting Eq. (A7) into Eq. (28), we have

$$\Delta\theta_m = \Delta\theta \cos\delta_2\left[1 - 2\cos 2\theta \sin\phi \times \left(\frac{z_0''}{z_0'}\sin\phi + \frac{y_0}{z_0'}\cos\phi\right)\right] - \Delta\phi\left[\cos\delta_2 \sin 2\theta\left(\frac{z_0''}{z_0'}\sin 2\phi + \frac{y_0}{z_0'}\cos 2\phi\right) + \sin\delta_2\left(\frac{z_0''}{z_0'}\cos 2\phi - \frac{y_0}{z_0'}\sin 2\phi\right)\right]. \quad \text{(A8)}$$

Equations (A6) and (A8) are Eqs. (31) and (32), respectively.

References

1. X. Dai, O. Sasaki, J. E. Greivenkamp, and T. Suzuki, "Measurement of small rotation angles by using a parallel interference pattern," Appl. Opt. **34,** 6380–6388 (1995).
2. J. G. Marzolf, "Angle measuring interferometer," Rev. Sci. Instrum. **35,** 1212–1215 (1964).
3. G. D. Chapman, "Interferometric angular measurement," Appl. Opt. **13,** 1646–1651 (1974).
4. P. Shi and E. Stijns, "Highly sensitive angular measurement with Michelson interferometer," Ind. Metrol. **1,** 69–74 (1990).
5. P. R. Yoder, Jr., E. R. Schlesinger, and J. L. Chickvary, "Active annular-beam laser autocollimator system," Appl. Opt. **14,** 1890–1895 (1975).
6. F. J. Schuda, "High-precision, wide-range, dual-axis, angle monitoring system," Rev. Sci. Instrum. **54,** 1648–1652 (1983).
7. O. Sasaki, K. Takahashi, and T. Suzuki, "Sinusoidal phase modulating laser diode interferometer with a feedback control system to eliminate external disturbance," Opt. Eng. **29,** 1511–1515 (1990).
8. O. Sasaki, H. Sasazaki, and T. Suzuki, "Two-wavelength sinusoidal phase-modulating laser-diode interferometer insensitive to external disturbances," Appl. Opt. **30,** 4040–4045 (1991).